JOURNAL OF COMPUTATIONAL PHYSICS 62, 414–428 (1986)

Adiabatic Particle Hydrodynamics in Three Dimensions*

MICHAEL LOEWENSTEIN AND WILLIAM G. MATHEWS

Lick Observatory and Board of Studies in Astronomy and Astrophysics, University of California, Santa Cruz, California 95064

Received April 10, 1984; revised March 11, 1985

A version of smoothed particle hydrodynamics, a method first developed by Lucy, Gingold and Monaghan, and Wood, is applied to three-dimensional adiabatic flows both with and without shocks. Results of such numerical experiments with $N \sim 10^2$ particles agree quite well with analytic results for the temperature as well as for the density and velocity provided that, for the shock tube problem, the proper artificial viscosity, Q, is used. Various forms of Q are discussed in terms of their effectiveness in damping out unphysical, non-systematic particle motions. The treatment of boundary conditions and the "biased point" correction are also discussed. The results are comparable in accuracy with the one-dimensional calculations of Monaghan and Gingold.

I. INTRODUCTION

Particle methods are often computationally superior to methods involving spatial grids when computing highly asymmetric three-dimensional gas-dynamical flows. The technique of employing a quasi-random distribution of particles to simulate local hydrodynamic variables has been extensively discussed in the recent literature [1–6, and references therein] and has been found to be both reasonably accurate and computationally efficient.

Until recently, almost all calculations using smoothed particle hydrodynamics (SPH) have involved isothermal flows, but Monaghan and Gingold [7, referred to here as MG, 8] have demonstrated that the SPH method can be extended to adiabatic flows in which each representative particle is endowed with an additional thermal parameter–temperature, specific internal energy, or entropy–in addition to its velocity which characterizes the local hydrodynamic flow velocity. As a test of the adiabatic SPH method, the shock tube problem was solved by MG with high accuracy, including a reasonably sharp shock transition. The shock width in this 1D calculation was governed by a new type of artificial viscosity which is sensitive to the random motion among the representative particles and which simulates some aspects of bulk viscosity.

The SPH calculation described by MG is strictly one-dimensional, as if all the representative particles were constrained to move along a wire. But it is clear that the real value of SPH as a computational tool lies in its application to two- and

* Lick Observatory Bulletin 1005.

0021-9991/86 $3.00

three-dimensional problems. We discuss here a truly three-dimensional adiabatic SPH scheme using only ~ 100 particles which accurately describes the one-dimensional adiabatic blowoff and steady adiabatic shocks of various strengths.

SPH shocks in three dimensions present a number of new problems. We have independently developed an artificial viscosity which is sensitive to the local peculiar velocity of representative particles. Random particle motions, which are particularly important within and behind shock transitions, must be properly damped and successfully converted into the hydrodynamic thermal parameter that labels each particle. In terms of the mean interparticle separation, our shocks in 3D are comparable to or sharper than those in 1D described by MG.

The conditions specified at the boundary are especially important to the success of 3D SPH calculations. The (smoothed) density evaluated at a particular particle must be corrected for the influence of fluid beyond the flow region as well as the "biased-point" correction described by Wood [5]. We derive this correction for both 1D and 3D gaussian and exponential smoothing functions and discuss the limitations imposed on the total number of representative points used in a 3D calculation.

II. Equations

In smoothed particle hydrodynamics, the flow variables at $\mathbf{r}$ are regarded as a smoothed local average:

$$(\rho(\mathbf{r})\, f(\mathbf{r}))_s = \int W(\mathbf{r}-\mathbf{r}')\, \rho(\mathbf{r}')\, f(\mathbf{r}')\, d\mathbf{r}' \approx \frac{M}{N} \sum_{j=1}^{N} f(\mathbf{r}_j)\, W(\mathbf{r}-\mathbf{r}_j), \tag{1}$$

where $f(\mathbf{r})$ is a (scalar or vector) flow variable, and the smoothing function W is normalized to unity when integrated over all space. Normally, continuous flow variables–density, temperature, or magnetic field, for example–are regarded as being localized at N "particles" that move with the fluid flow. Assuming these particles to be randomly distributed, the integral in Eq. (1) is approximated by a weighted sum over values stored at nearby points. The factor $\rho(\mathbf{r}')/M$ serves as a convenient normalized probability distribution in this Monte Carlo approximation, where M is the total mass of all the particles. Furthermore, approximation of flow variables as in Eq. (1) can be considered as a special case of interpolation by kernel estimation. This leads to a systematic procedure for deriving SPH equations from the standard equations of hydrodynamics [6].

In Lagrangian hydrodynamics, it is necessary to establish values of the smoothed variables at a particular (the kth) particle. An appropriate smoothing function should therefore depend only on the interparticle distance, $r_{jk} = |\mathbf{r}_j - \mathbf{r}_k|$. We adopt, following Wood [5], an exponential form:

$$W(r_{jk}) = \frac{1}{8\pi h_k^3}\, e^{-r_{jk}/h_k}. \tag{2}$$

The choice of kernel is, in principle, arbitrary. The exponential kernel differs from the gaussian kernel, as explored extensively by Gingold and Monaghan, in that (1) it has no maximum, a quality which may help avoid secondary structures [4], and (2) since it falls off more slowly with r/h a somewhat higher resolution (smaller h) can be utilized.

With this smoothing function, the sum in Eq. (1) can be written as

$$\rho_k f_k = \frac{M}{8\pi h_k^3}\left[f(r_k)(1-A(l)) + \sum_{j\neq k} f(r_j) e^{-r_{jk}/h_k} \right], \tag{3}$$

where $A(l)$, discussed below, corrects for the biased choice of the position of the kth particle as one of the random points for the Monte Carlo integration [5], and for proximity to boundaries. The smoothing length, h_k, is given by

$$h_k = \lambda_k / l,$$

where λ_k is the mean interparticle separation at the position of the kth particle, $(N\rho_k/M)^{-1/3}$. The ratio of mean interparticle separation to smoothing length, l, is taken to be constant. We use Eq. (3) to determine the density ρ_k for which $f=1$, and the internal energy density $(\rho\mathscr{E})_k$, for which $f=\mathscr{E}$ (ergs per gram).

The equation of motion for the kth particle is

$$\frac{d\mathbf{u}_k}{dt} = -\frac{2[\nabla(\rho\mathscr{E})]_k}{3\rho_k} - \left[\frac{\nabla Q}{\rho}\right]_k \equiv \mathbf{A}_k, \tag{5}$$

where

$$[\nabla(\rho\mathscr{E})]_k = \frac{M}{8\pi N h_k^4} \sum_{j\neq k} \mathscr{E}(r_j)\, \hat{r}_{jk}\, e^{-r_{jk}/h_k}, \tag{6}$$

and $\hat{r}_{jk}$ is the unit vector $(\mathbf{r}_j - \mathbf{r}_k)/r_{jk}$. The artificial viscosity Q is discussed below. Note that the flow (or particle) velocity $\mathbf{u}_k$ is not a locally smoothed quantity like ρ_k and $(\rho\mathscr{E})_k$.

In addition to position $\mathbf{r}_k$ and velocity $\mathbf{u}_k$, in adiabatic flow each particle is endowed with a specific internal energy $\mathscr{E}_k$ which is determined by an energy equation

$$\frac{d\mathscr{E}_k}{dt} = \left[\frac{2\mathscr{E}_k}{3\rho_k} + \left(\frac{Q}{\rho^2}\right)_k\right]\left(\frac{d\rho}{dt}\right)_k \equiv G_k \left(\frac{d\rho}{dt}\right)_k. \tag{7}$$

In both space and time derivatives we ignore variations of h_k.

Equations (5) and (7) along with $\mathbf{u}_k = d\mathbf{r}_k/dt$ provide $7N$ equations for solving general adiabatic gas flow including shocks; the conservation of mass is automatically satisfied by the conservation of particles. Following Gingold and

Monaghan [3], we use a simple explicit leap frog scheme to calculate time-advanced quantities:

$$\begin{aligned}\mathbf{u}_k^{n+1/2} &= \mathbf{u}_k^{n-1/2} + \tfrac{1}{2}(\Delta t^{n+1/2} + \Delta t^{n-1/2})\,\mathbf{A}_k^n \\ \mathbf{r}_k^{n+1} &= \mathbf{r}_k^n + \Delta t^{n+1/2}\mathbf{u}_k^{n+1/2}, \\ \mathscr{E}_k^{n+1} &= \mathscr{E}_k^n + G_k^{n+1/2}(\rho_k^{n+1} - \rho_k^n).\end{aligned} \tag{8}$$

The time-advanced densities ρ_k^{n+1} can be found directly from the $\mathbf{r}_k^{n+1}$ and Eq. (3). It is sufficiently accurate to evaluate the smoothing parameter h_k in terms of densities at the retarded time, ρ_k^n. The time step is limited by a modified Courant condition:

$$\Delta t = \mathrm{Min}\left[a_1 \frac{h_k}{|\mathbf{u}_k|}, a_2 \frac{h_k}{c_{sk}}, a_3 \left(\frac{h_k}{|\mathbf{A}_k|}\right)^{1/2}\right], \tag{9}$$

where $c_{sk} = (10\mathscr{E}_k/9)^{1/2}$ is the local sound speed and a_1, a_2, and a_3 are dimensionless coefficients of order unity.

A. The Correction $\Lambda(l)$

The mean interparticle distance among N particles is $\lambda = (V/N)^{1/3}$, whe $V = L^3$ is the characteristic volume of the flow region. Generally, when $l \equiv \lambda/h$ is less than unity, the approximation for $\rho_k f_k$ given by Eq. (3) with $\Lambda = 0$ is excellent aside from boundary effects (see below).

However, $l = N^{-1/3}/(h/L)$ can exceed unity if high resolution of the flow variables, $h \ll L$, is required with fixed N. For example, if $N = 100$ and $h/L < 0.1$, then $l \geqslant 2.15$. As noted by Wood [5] the smoothed density ρ_s will be overestimated for large values of l due to the enhanced contribution of the kth particle to the sum in Eq. (3). A correction term, $\Lambda(l)$, proportional to $(\rho_s - \rho)/\rho$ is useful to adjust ρ_s to the true density ρ of a locally uniform medium.

The correction $\Lambda(l)$ can be estimated by assuming that the mass points are arranged in a uniform lattice [5]. The appropriate corrections for one (1D) and three (3D) dimensional grids are

$$\Lambda_E^{(3D)} = -8\pi/l^3 + \sum_{i,j,k=-\infty}^{\infty} e^{-(i^2+j^2+k^2)^{1/2} l},$$

$$\Lambda_G^{(3D)} = -\pi^{3/2}/l^3 + \sum_{i,j,k=-\infty}^{\infty} e^{-(i^2+j^2+k^2) l^2},$$

$$\Lambda_E^{(1D)} = -2/l + \sum_{i=-\infty}^{\infty} e^{-il} = \left(\frac{e^l+1}{e^l-1}\right) - 2/l,$$

TABLE I

Values of $\Lambda_E^{(1D)}$ and $\Lambda_E^{(3D)}$

l \ I	1D	3D	3D			
	∞	∞	4	3	2	R
0.5	0.083	0.121	−31.97	−55.47	−91.99	−94.50
1.0	0.164	0.259	0.010	−0.623	−2.69	−7.29
1.5	0.241	0.378	0.375	0.351	0.194	−0.298
2.0	0.313	0.484	0.484	0.483	0.469	0.723
2.5	0.378	0.577	0.577	0.577	0.576	0.917
3.0	0.438	0.655	0.655	0.655	0.655	0.949

and

$$\Lambda_G^{(1D)} = -\pi^{1/2}/l + \sum_{i=-\infty}^{\infty} e^{-i^2 l^2},$$

where the subscripts refer to properly normalized exponential or gaussian smoothing functions. Values of Λ are listed in the $I=\infty$ column of Tables I and II. In the three-dimensional calculations described below we have employed the exponential kernel $W_E^{(3D)}$ with $l=2.5$ fixed throughout the calculation; this provides a resolution of $h/L \sim 0.09$ for $N \sim 100$. We therefore adopt a correction $\Lambda_E^{(3D)} = 0.576$ in Eq. (3) when the particle distributions are relaxed (see below). Wood's approximation $\Lambda_E^{(3D)} \sim erf(l/2\pi^{1/2})$ overestimates $\Lambda_E^{(3D)}$ by about 20% at $l=2.5$. In MG's 1D calculation, which employed 400 particles, $h=0.015$ was fixed and $l=0.1-0.5$ was sufficiently small that no explicit correction was required, i.e, $\Lambda_G^{(1D)} = 0.0$. In 3D calculations, it is more difficult to ensure $l \leqslant 1$, and the correction $\Lambda^{(3D)}$ provides a significant improvement.

An additional modification to this biased-point correction may be required if the

TABLE II

Values of $\Lambda_G^{(1D)}$ and $\Lambda_G^{(3D)}$

l \ I	1D	3D	3D		
	∞	∞	4	3	2
0.5	0.000	0.000	0.000	-0.0178	-0.641
1.0	0.000	0.002	0.002	0.002	0.002
1.5	0.0294	0.126	0.126	0.126	0.126
2.0	0.150	0.418	0.418	0.418	0.418
2.5	0.295	0.655	0.655	0.655	0.655
3.0	0.409	0.794	0.794	0.794	0.794

kth particle is too close to a boundary of the flow. If particles beyond the boundary do not contribute to the sum in Eq. (3), $\rho_k f_k$ will be underestimated and $\Lambda(l)$ must be reduced. In the flow problems described below, we assume periodic boundary conditions in two cartesian directions perpendicular to the flow, requiring that two of the sums for $\Lambda_E^{(3D)}$ be restricted to $|i|, |j| \leqslant I$. For example, for $N=125$, $2I+1=5$, so $I=2$ is appropriate for the midpoint of a 5×5 grid perpendicular to the flow. Values of $\Lambda_E^{(3D)}$ and $\Lambda_G^{(3D)}$ are provided in Tables I and II for $I=2$, 3, and 4. For our value $l=2.5$, $\Lambda_E^{(3D)}$ is not appreciably different from its $I=\infty$ value. However, for $l \leqslant 1$, the corrections to $\rho_k f_k$ can be unacceptably large. When $l \geqslant 1$, $\Lambda(l)$ tends to be independent of I since fewer particles lie within the smoothing distance h, but Λ can be large in this situation. As can be seen by examining the expressions for Λ in one dimension, the gaussian kernel, $W_G^{(1D)}$ always requires less of a correction than the exponential kernel, $W_E^{(1D)}$. This is also the case in three dimensions for $l \leqslant 1$. However, the function ρ_s/ρ diverges much faster when $l \geqslant 1$ for $W_G^{(3D)}$ than it does for $W_E^{(3D)}$. For example, when $l=2$ ρ_s/ρ is 1.15 and 1.60 for $W_E^{(3D)}$ and $W_G^{(3D)}$, respectively, while for $l=2.5$ the respective values are 1.36 and 2.83. Thus 3D calculations with a gaussian kernel can provide a particularly poor approximation to ρf when $l \geqslant 1$ which can arise if h is fixed and the flow density drops to low values. Finally, we note that for fixed N and L, l must be smaller by about 0.4 when using $W_G^{(3D)}$ than for $W_E^{(3D)}$ to incorporate the same number of local particles within the half width of the smoothing function.

We have chosen $W_E^{(3D)}$ as the smoothing function rather than $W_G^{(3D)}$ because of the improved accuracy of $W_E^{(3D)}$ for larger l, its demonstrated success in representing the density in previous calculations, and the guaranteed resistance of $W_E^{(3D)}$ to spurious particle clustering [4].

III. The Rarefaction Wave

Our first test of the 3D adiabatic SPH method is to consider the problem of the abiabatic ($\gamma=5/3$) one-dimensional free expansion into a vacuum. The initial configuration is set up by choosing the positions of the particles at random in a box then allowing them to relax isothermally under an equation of motion with damping:

$$\frac{d\mathbf{u}_k}{dt} = -\frac{2}{3}\frac{\rho_0}{\rho_k}\frac{V}{8\pi N h_0^4}\mathscr{E}_0 \sum_{j\neq k} e^{-r_{jk}/h_0}\hat{\mathbf{r}}_{jk} - \frac{\mathbf{u}_k}{\tau}; \qquad k=1, N.$$

Here $\mathbf{u}_k$ is the velocity of the kth particle, N is the number of particles, V the volume of the box, $\rho_0 = M/V$, where M is the total mass of all particles, and $\mathscr{E}_0$ is the initial specific internal energy. Boundary conditions are strictly periodic in all three directions during the damping transient. All particles have identical smoothing lengths h_0 during the damping preparation:

$$h_0 = \frac{1}{l}\left(\frac{N}{V}\right)^{-1/3},$$

and the damping time τ is chosen to be $0.1\ h_0 a_0/\mathscr{E}_0$, in which a_0 is the initial adiabatic sound speed. Fluctuations in the density are reduced by this method until the variance $N^{-1}\sum(\rho_k/\rho_0 - 1)^2$ is about 1%. The damped and very subsonic residual velocities are reset to zero prior to the blowoff calculation.

We invoke periodic boundary conditions in the two directions perpendicular to the one dimensional flow. Although the physical flow is entirely in the x-direction, individual particles may acquire y and z velocity components. Should particles pass through a y or z wall, they re-enter the volume V from the opposite wall. In addition, when smoothing the flow variables, each particle is treated on an equal footing by considering it as being located at the origin of the y, z coordinates interacting with particles or their images consistent with the periodic boundary conditions and the y, z box dimensions. In the x-direction, one boundary is free, but a correction must be applied to the opposite boundary to simulate the existence of a semi-infinite region of uniform density ρ_0 and thermal energy $\mathscr{E}_0$. If the kth particle is located a distance ηh_k from this uniform region, the corrections to the density and acceleration are

$$\delta\rho_k = \int \rho_0 W(\mathbf{r}_k - \mathbf{r}')\, d\mathbf{r}' = \frac{\rho_0}{4}(\eta + 2)\, e^{-\eta}$$

and

$$\delta\mathbf{A}_k = -\frac{2}{3\rho}\int \nabla_k(\rho_0 \mathscr{E}_0 W(\mathbf{r}_k - \mathbf{r}'))\, d\mathbf{r}' = \frac{\mathscr{E}_0 \rho_0}{6\rho_k h_k}(\eta + 1)\, e^{-\eta}\hat{x},$$

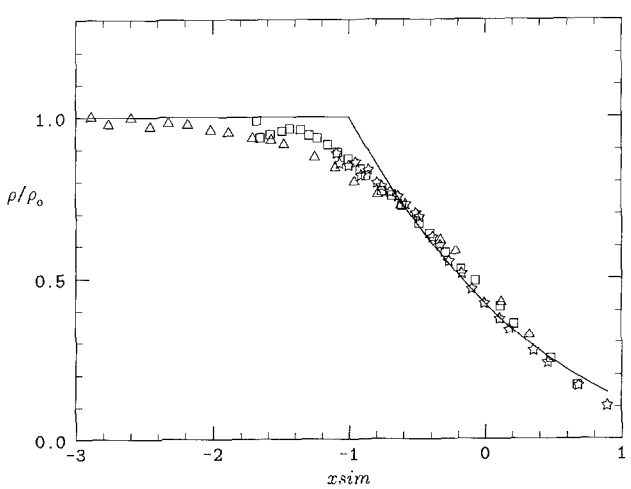

FIG. 1. Results for the adiabatic rarefaction wave for density with $N = 125$ plotted versus the similarity variable $x_{\text{sim}} = (x - L_x)/a_0 t$. Triangles represent time $= 0.29$, boxes time $= 0.58$, and stars time $= 0.89$. Times are in units of the sound crossing time, $2L_x/a_0$.

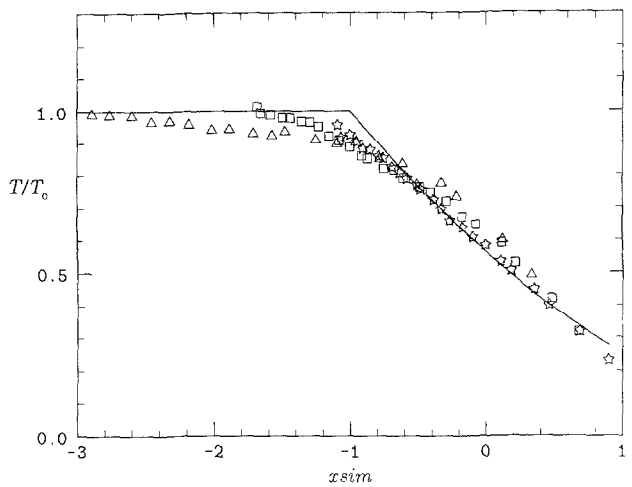

FIG. 2. Results for the adiabatic rarefaction wave for temperature plotted in the same manner as the density.

where the integration is over the uniform semi-infinite region. These corrections prevent an unphysical density drop and pressure gradient near the boundary. A fixed boundary can also be simulated by imposing reflection symmetry in which each particle is repulsed from its image at the boundary. Results for the rarefaction wave were similar using either of these boundary conditions.

The density, temperature, and velocity for the computed adiabatic rarefaction wave are shown in Fig. 1–3. Here $l=2.5$, $Q=0$, and $N=125$ particles are con-

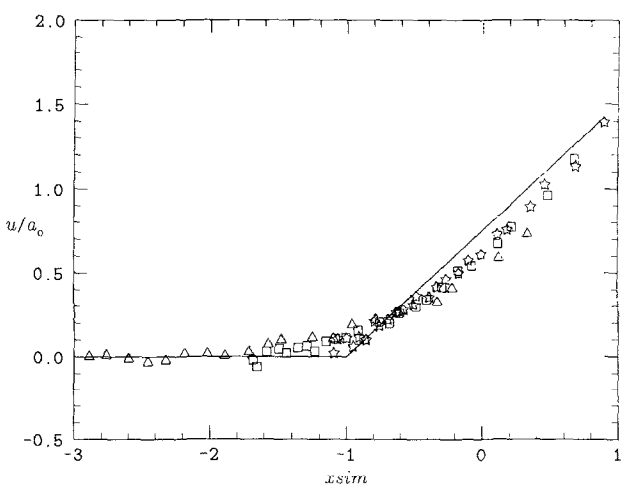

FIG. 3. Results for the adiabatic rarefaction wave for velocity plotted in the same manner as the density.

sidered in a box of dimensions $L_x : L_y : L_z :: 2 : 1 : 1$. Exploiting the self-similar nature of the problem, we plot the x-variation of flow variables at various times superimposed as functions of the similarity variable $x_{\text{sim}} = (x - L_x)/a_0 t$. Times are in units of the sound crossing time $2L_x/a_0$. To avoid confusion, each point in Fig. 1–3 represents the average of a bin of five particles. In the undisturbed medium ahead of the rarefaction wave, the mean particle separations in units of the similarity variable are 0.43, 0.22, and 0.14 for times 0.29, 0.58 and 0.89, respectively. The weak discontinuity at the head of the rarefaction wave is smoothed over several interparticle separations due to the finite resolution of the SPH method. At the earliest times, $t \leqslant 0.3$ or so, inaccuracies result from the rather small number of particles participating in the flow. For $t \geqslant 1$, the computed rarefaction wave interacts with the fixed boundary and similarity no longer applies. Apart from this, the results are in excellent agreement with the expected flow.

IV. Steady Shock

The initial configuration for a standing shock is arranged by choosing particles randomly in the y, z-plane and as random samples of the probability distribution

$$P(x) = \rho_1/\rho_0, \qquad -L_x \leqslant x < 0;$$
$$P(x) = \rho_2/\rho_0, \qquad 0 \leqslant x \leqslant L_x$$

in the x-direction [9]. As before, $\rho_0 = M/V$. The pre-shock and post-shock sides are relaxed separately at constant h_0 and $\mathscr{E}_0$, although unrelaxed, purely random particles are introduced once the calculation begins. Initially, velocities, internal energies, and smoothing lengths appropriate to the position of each particle are assigned in accordance with the expected jump conditions of the shock under consideration. Following an initial transient, as the shock front widens by several h, the flow becomes steady again establishing the computed jump conditions.

As before, the boundary conditions are periodic in the y- and z-directions. In the x-direction, the density and acceleration are corrected for the effects of two semi-infinite uniform flows on both sides of the shock;

$$\delta\rho_k = \frac{1}{4}\frac{\rho_2}{\rho_0}\left[\frac{\rho_1}{\rho_2}(\eta_1 + 2)\, e^{-\eta_1} + (\eta_2 + 2) e^{-\eta_2}\right],$$

and

$$\delta\mathbf{A}_k = \frac{\mathscr{E}_2}{6h_k}\frac{\rho_2}{\rho_k}\left[\frac{\mathscr{E}_1\rho_1}{\mathscr{E}_2\rho_2}(\eta_1 + 1)\, e^{-\eta_1} + (\eta_2 + 1)\, e^{-\eta_2}\right]\hat{x},$$

where $h_k\eta_1$ and $h_k\eta_2$ are the distances to the embedding media with uniform ρ_1, $\mathscr{E}_1$ and ρ_2, $\mathscr{E}_2$. Once the calculation begins, particles are introduced into the pre-shock

flow at regular rate to keep the total number of particles N essentially constant, but the particle input rate must be independent of the post-shock outflow rate to avoid feedback effects.

The shock structure in SPH is characterized by strong cross-streaming among the representative particles. Such relative motions represent an unrealized thermal energy which must be converted into thermal energy at each particle by means of a properly defined artificial viscosity Q. We have considered three types of artificial viscosity. The first is equivalent to the von Neumann–Richtmyer viscosity,

$$Q^{(1)} = (a\,\Delta x)^2\,\rho(\nabla\cdot\mathbf{u})^2, \qquad \nabla\cdot\mathbf{u}<0;$$
$$Q^{(1)}=0, \qquad \nabla\cdot\mathbf{u}>0,$$

where Δx is the local grid size and a is a parameter of order unity. In the smoothed particle realization of this viscosity, we replace Δx with the smoothing length h and evaluate $\nabla\cdot\mathbf{u}$ with $(\nabla\cdot\rho\mathbf{u}-\mathbf{u}\cdot\nabla\rho)/\rho$ following MG. For the kth particle

$$\frac{Q_k^{(1)}}{\rho_0}=\frac{\rho_0}{\rho_k}\left(\frac{aV}{8\pi N h_k^3}\right)^2\left[\sum_{j\neq k}(\mathbf{u}_k-\mathbf{u}_j)\cdot\mathbf{r}_{jk}\,\Delta_{jk}e^{-r_{jk}/h_k}\right]^2,$$

where

$$\Delta_{jk}=1, \qquad (\mathbf{u}_j-\mathbf{u}_k)\cdot\mathbf{r}_{jk}<0;$$
$$\Delta_{jk}=0, \qquad (\mathbf{u}_j-\mathbf{u}_k)\cdot\mathbf{r}_{jk}>0,$$

assures that only particles converging toward the kth particle contribute to the local artificial viscosity, a technique also employed by MG.

Second, we considered an artificial viscosity in the form of a pressure based on the peculiar velocity of the kth particle relative to its neighbors,

$$\frac{Q_k^{(2)}}{\rho_0}=\frac{aV}{8\pi N h_k^3}\sum_{j\neq k}(\mathbf{u}_k-\mathbf{u}_j)^2\,e^{-r_{jk}/h_k}\,\Delta_{jk}.$$

A third type of viscosity is specifically designed to damp out random velocities in the shock region,

$$\frac{Q_k^{(3)}}{\rho_0}=\frac{aV}{8\pi N h_k^3}\sum_j(\mathbf{u}_j-\langle\mathbf{u}\rangle_j)^2\,e^{-r_{jk}/h_k},$$

where $\langle u\rangle_k$ is the local mean velocity at the position of the kth particle,

$$\langle\mathbf{u}\rangle_k=\frac{V}{8\pi N h_k^3}\frac{\rho_0}{\rho_k}\left[\sum_{j\neq k}\mathbf{u}_j e^{-r_{jk}/h_k}+\mathbf{u}_k(1-A(l))\right]+\delta\mathbf{u}_k.$$

Here $\delta\mathbf{u}_k$ is a boundary correction similiar to $\delta\rho_k$ and $\delta\mathbf{A}_k$ above.

The artificial viscosity developed by MG contains, in addition to a, a second dimensionless control parameter ε such that $Q_{\mathrm{MG}} \propto (r_{ij}^2 + \varepsilon h^2)^{-1}$, where $0 < \varepsilon \leqslant 0.1$. This form of the artificial viscosity was used in a three-dimensional calculation by Gingold and Monaghan [8], but was largely justified on the basis of 1D considerations by MG. Evidently ε is required in strong compressions following 1D shocks (where no counterstreaming is possible) to avoid undesirably large values of Q_{MG}. In our three-dimensional calculation the post-shock condition is characterized by particles counterstreaming normal to the shock. Also our choice of an exponential kernel, rather than the gaussian employed by MG, enhances the pressure related mutual repulsion among the particles. Finally, MG note that ε must be a function of the Mach number for best results. We have nevertheless computed shocks comparable in quality to those of MG without using this additional parameter.

Momentum is more accurately conserved and the results generally better when an anti-symmetrical form for the gradient of the artificial viscosity is used in the equation of motion,

$$-\frac{\nabla Q}{\rho} = -\frac{Q}{\rho^2}\nabla\rho - \nabla\left(\frac{Q}{\rho}\right) = -\frac{V}{8\pi N h_k^4}\sum_{j\neq k}\left[\frac{Q_k/\rho_0}{(\rho_k/\rho_0)^2} + \frac{Q_j/\rho_0}{(\rho_j/\rho_0)^2}\right] e^{-r_{jk}/h_k}\hat{\mathbf{r}}_{jk}.$$

Computed results for a Mach 3 shock using 150 particles are shown in Figs. 4–6. The x-coordinate is in units of the half length of the box, and the density, temperature, and velocity are in units of the analytic values of variables in the pre-shock flow. On this scale the smoothing length is about 0.11 in the pre-shock flow and 0.087 in the post-shock flow. Time is in units of the expected flow time across

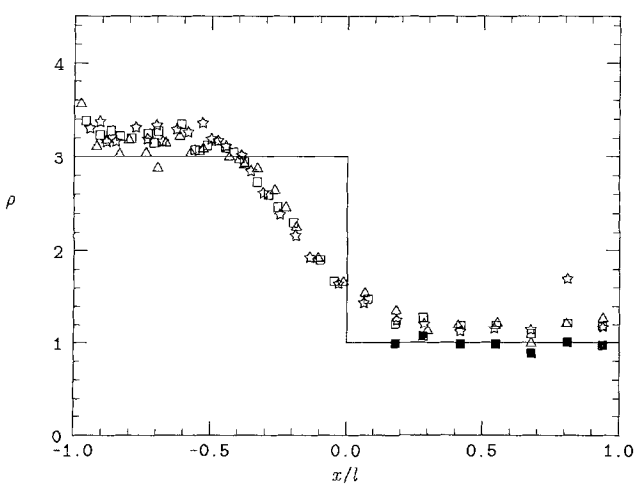

FIG. 4. Results with $N = 150$ for the Mach 3 steady state shock for density, plotted versus position in units of the box's half length. Triangles represent time $= 1.87$, empty boxes time $= 2.0$, and stars time $= 2.13$. Filled boxes represent the density with the modified correction discussed in the text.

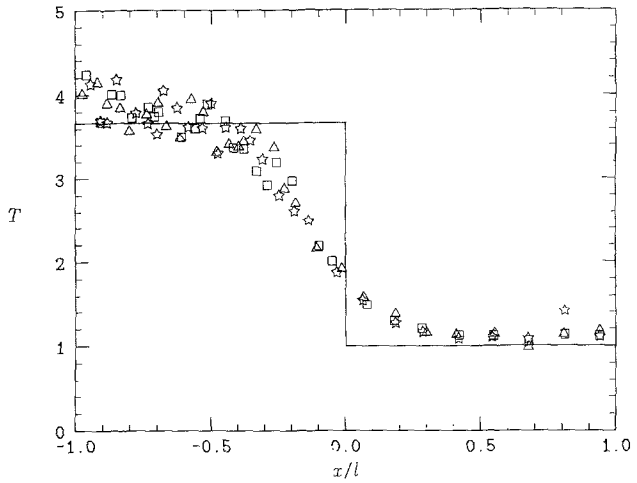

FIG. 5. Temperature variation with $N = 150$ for the Mach 3 steady state shock.

the entire box, $4L_x/3a_2$ where a_2 is the sound speed in the pre-shock flow. The three times illustrated are separated by 0.13 in these units. The results shown were calculated using the second form of the artificial viscosity discussed above with $a = 3.0$. Figure 7 shows the ratio of this viscosity to the local gas pressure. Comparison of the flow variables at several times indicates that the shock is quite steady. During the entire calculation energy is conserved to about 8% and momentum to about 5%. To avoid confusion, the particles are grouped in bins of five as

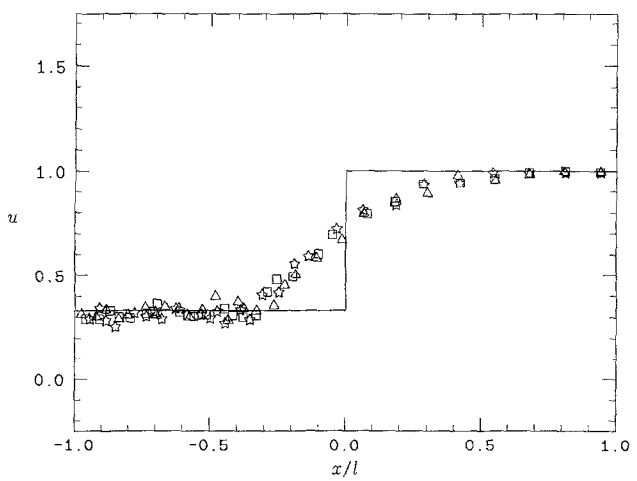

FIG. 6. Velocity variation with $N = 150$ for the Mach 3 steady state shock.

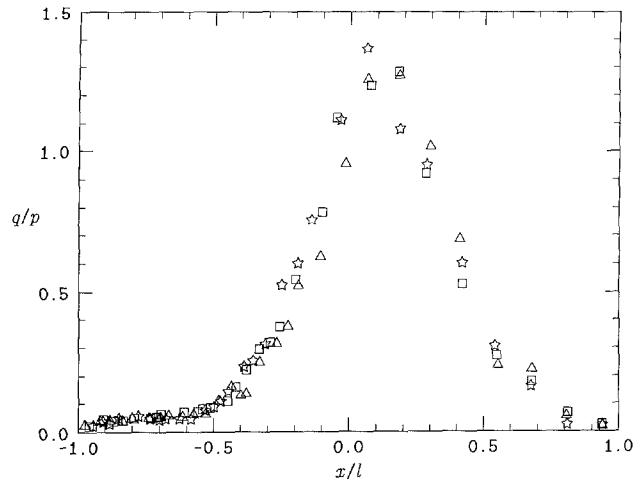

FIG. 7. The artificial viscosity divided by the pressure, $3Q/(2\rho\varepsilon)$ again plotted versus position in units of the box's half length for $N = 150$, Mach number $= 3$, using the second type of artificial viscosity with viscosity parameter $a = 3.0$.

before. We note that in all of our calculations, the fluctuations of the flow variables evaluated at individual neighboring particles in a bin is less than 10%.

As shown in Fig. 4, the density in the pre-shock flow is systematically high by about 20% at all times. In fact, however, the true density of particles in the pre-shock region, obtained by dividing the number of particles by the volume, is exactly correct. The misrepresentation in Fig. 4 is due to the fact that the particles are introduced into the box with random positions in the y- and z-directions. Purely random, unrelaxed particles have more close pairs than a lattice so that a larger $\Lambda(l)$ is required. This larger correction is illustrated in Table I under column R, which shows $\Lambda(l)$ calculated for a distribution of 150 particles with random positions in two of the three spatial directions. In Fig. 4, the filled-in squares represent the density with this correction for the same time as the open boxes. As expected, the true density lies somewhere between the filled and open boxes, but much nearer to the filled boxes. In the shock (and post-shock) region, the viscosity will tend to relax the particles toward a more widely spaced spatial distribution for which the standard correction $\Lambda_E^{(3D)}(l)$ should apply. Although we could have prepared a relaxed pre-shock particle distribution (as in Sect. 3), we chose to illustrate this additional correction explicitly. The shock width is approximately 7.5 smoothing lengths as compared to 3 smoothing lengths for the best results obtained by MG. However, the smoothing length is larger for our exponential kernel than for the gaussian kernel used by MG. A more physically appropriate means of comparing shock widths is in terms of the local mean particle separation λ. Our shock width is 3λ while that of MG is 5λ, which refers to a somewhat smaller Mach number. We find that the shock width is quite independent of the Mach number for

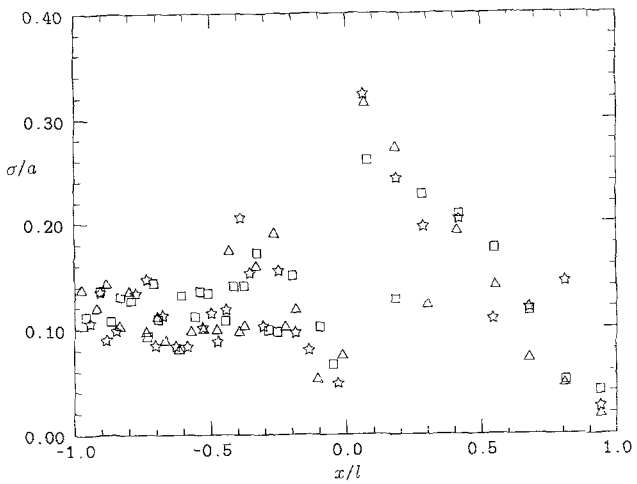

FIG. 8. Ratio of the velocity dispersion to local sound speed plotted versus position for the same shock calculation as above.

Mach numbers $\leqslant 3.0$, and independent of the coefficient a in the expression for $Q^{(2)}$ over the range $0.7 \leqslant a \leqslant 3.0$.

Figure 8 shows the velocity dispersion in each bin as a function of position and indicates the amount of energy contained in the random motion of the particles. The increasing particle motion in the pre-shock flow is due to the separation of close pairs of unrelaxed particles which are introduced at random in the y-z plane. Following the shock the particle dispersion is remarkably low. The post-shock particle velocity dispersion and other results using $Q^{(3)}$ (with $a = 5.0$) were comparable to those presented here for $Q^{(2)}$, but $Q^{(1)}$ was significantly less effective in damping particle motions across the shock, with the result that the post-shock temperature was too low (by 20% or more) and the post shock density was necessarily higher to achieve overall pressure balance across the shock. This effect is also present in Figs. 4 and 5, but the post-shock density and temperature are within 10% of the expected values. These difficulties with $Q^{(1)}$ were less troublesome at low Mach numbers. Post-shock oscillations of the sort found by MG for a viscosity analogous to $Q^{(1)}$ were not found in our study and are evidently an artifact of the one-dimensional geometry used by MG.

V. CONCLUSIONS

The results of our calculations show that the smoothed particle method can be extended to three-dimensional adiabatic flows which may possibly develop shocks. We have obtained accurate results for an adiabatic rarefaction wave, as well as for a steady state shock using a simple first order integration scheme and a very modest

number of particles ($\sim 10^2$). Shock widths are about three mean particle separations, comparable to the one-dimensional results of MG. At the shock, systematic kinetic particle motion will be converted to three-dimensional counter-streaming and random particle motion. This represents an unrealized temperature which must be converted to thermal energy using an appropriate form of the artificial viscosity in order to obtain the proper jump conditions across the shock. Finally, great care must be taken at the locations of boundaries in the flow, and the proper biased point correction must be applied when using smoothed particle methods in three dimensions. Our work, and that of Wood, demonstrates that the correct density can be well approximated with a correction based on a uniform lattice distribution; this is not particularly obvious and may be regarded as an empirical result of our test calculations.

To those experienced in computational hydrodynamics, the shocks calculated here may seem rather crude. However, it must be stressed that ours is a fully three-dimensional calculation and that the shock structure incorporates remarkable few particles. To achieve the same accuracy with a conventional grid approach, one would require about ten zones across the region shown in Figs. 4–8. The entire 3D grid would then consist of approximately $10 \times 5 \times 5 = 250$ zones, comparable or somewhat larger to the 150 particles considered here. When viewed from this perspective, 3D particles methods provide an accuracy comparable to standard grid codes for the same expenditure of CPU time. They are also free of the many difficulties specific to three-dimensional grid procedures.

Finally we note that if the total number of particles N were increased, the rarefaction and shock waves would be sharper in physical space, but their widths in terms of the mean particle separation λ would remain the same. For this reason, an economical calculation with small N, as described above, is sufficient to test the numerical procedure.

ACKNOWLEDGMENTS

It is a pleasure for us to acknowledge support from the California Space Institute and the National Science Foundation (AST83–12971).

REFERENCES

1. L. B. LUCY, *Astron. J.* **82** (1977), 1013.
2. R. A. GINGOLD AND J. J. MONAGHAN, *Mon. Not. R. Astron. Soc.* **181** (1977), 375.
3. R. A. GINGOLD AND J. J. MONAGHAN, *J. Comput. Phys.* **46** (1982), 429.
4. M. SCHÜSSLER AND D. SCHMITT, *Astron. Astrophys.* **97** (1981), 373.
5. D. WOOD, *Mon. Not. R. Astron. Soc.* **194** (1981), 201.
6. J. J. MONOGHAN, *SIAM J. Sci. Statist. Comput.* **3** (1982), 422.
7. J. J. MONAGHAN AND R. A. GINGOLD, *J. Comput. Phys.* **52** (1983), 375.
8. R. A. GINGOLD AND J. J. MONAGHAN, *Mon. Not. R. Astron. Soc.* **204** (1983), 715.
9. J. M. DAWSON, *Rev. Mod. Phys.* **55** (1983), 403.